MODERN ASPECTS OF ELECTROCHEMISTRY, No. 48:

ELECTRODEPOSITION

THEORY AND PRACTICE

For other titles published in this series, go to
www.springer.com/series/6251

Modern Aspects of Electrochemistry

Series Editors:
Ralph E. White
Department of Chemical Engineering
University of South Carolina
Columbia, SC 29208

Constantinos G. Vayenas
Department of Chemical Engineering
University of Patras
Patras 265 00
Greece

Managing Editor:
Maria E. Gamboa-Aldeco
1107 Raymer Lane
Superior, CO 80027

MODERN ASPECTS OF ELECTROCHEMISTRY, No. 48:

ELECTRODEPOSITION

THEORY AND PRACTICE

Edited by

Stojan S. Djokić
Elchem Consulting Ltd., Canada

Springer

Editor
Dr. Stojan S. Djokić
Elchem Consulting Ltd.
15511-103 Street NW.
Edmonton AB T5X 6B3
Canada
sdjokic@telus.net

ISBN 978-1-4419-5588-3 e-ISBN 978-1-4419-5589-0
DOI 10.1007/978-1-4419-5589-0
Springer New York Dordrecht Heidelberg London

Library of Congress Control Number: 2010925320

Preface

In the past few decades, research in the electrochemical and chemical deposition of metals, alloys, and compounds has brought about significant achievements that are important for the practical applications. The research in this area was related and/or supported with the developments in electronics, aerospace, automotive, energy conversion, and biomedical industries.

The aim of this issue of Modern Aspects of Electrochemistry is to review the latest developments in the science of electrochemical and chemical deposition of various metals, alloys, and/or compounds.

Competent scientists/researchers in their respective fields from all around the world were invited to write this volume and I am very thankful to them to make this volume a reality.

Nikolić and Popov in Chapter 1 discuss the effects of codeposition of hydrogen on the structure of electrodeposited copper. The simultaneous hydrogen evolution and codeposition is more extensively studied in the cases of electrodeposition of chromium or iron group of metals and/or alloys. An increased hydrogen evolution during the electrodeposition of metals leads to noticeable changes in mass and heat transfer, limiting current density, and Ohmic resistance. Consequently, the simultaneous hydrogen evolution significantly influences the surface morphology of the deposited copper, thus leading to the formation of open porous structure with extremely high surface area. The honeycomb-like or other different features of the surface morphology as well as various shapes of electrochemically prepared powders are correlated to the amount of simultaneously evolved hydrogen during the electrodeposition process. From a practical point of view, due to extremely high surface area, materials prepared in this way can be technologically very useful for the applications as electrodes in fuel cells, batteries, or sensors.

Chapter 2, by Štrbac and Wieckowski, gives an impressive overview of a new class of electrode materials that deserve an advanced focus in the future. This chapter is related to the electrochemical or spontaneous deposition of Ru and Os on Au(111) and Pt(111) single crystal surfaces. The contribution of this chapter is particularly important for the understanding of the principles of reactivity

at single crystal electrodes modified by metal nanoislands in the heterogeneous catalysis research. On the applied side, the authors correlate the surface structure and its catalytic activity with the reactions relevant for the fuel cells.

In Chapter 3, by Shaigan, electrodeposition for electrochemical conversion and storage devices is presented. This chapter discusses the latest developments on metal, metal oxide, and conductive polymer electrodeposition processes developed and studied for the applications in the fields of fuel cells, batteries, and capacitors. The importance of electrodeposited materials, which are used or may have the future potential applications in the energy conversion or storage, is clearly shown.

In Chapter 4 by Popov et al., the aspects of the newest developments of the effect of surface morphology of activated electrodes on their electrochemical properties are discussed. These electrodes, consisting of conducting, inert support which is coated with a thin layer of electrocatalyst, have applications in numerous electrochemical processes such as fuel cells, industrial electrolysis, etc. The inert electrodes are activated with electrodeposited metals of different surface morphologies, for example, dendritic, spongy-like, honeycomb-like, pyramid-like, cauliflower-like, etc. Importantly, the authors correlate further the quantity of a catalyst and its electrochemical behavior with the size and density of hemispherical active grain.

Brevnov and Mardilovich present in Chapter 5 the electrochemical micromachining and surface microstructuring based on porous-type anodization of patterned films. Anodic dissolution of aluminum in unprotected areas results in the formation of the porous Al_2O_3 features, whose trapezoidal shape is dictated by the ratio of the vertical and lateral dissolution rates. On the other hand, in the areas protected by the anodization mask, the Al phase is preserved. As a result, the obtained microstructure represents a combination of regions of Al and Al_2O_3. Micro- and nanostructured Al and Al_2O_3 substrates can be used as templates in soft lithography. This aspect of surface treatment is very important for applications in the microelectronics and solar cell industries as well in the fabrication of passive electrical components. The review further focuses on the technological merits of these microfabrication methods and their application for fabrication of 3D metallic and ceramic microstructures.

Djokić and Cavallotti in Chapter 6 discuss the latest developments in the field of electroless deposition. This review is

complementary to Djokić's chapter published in Modern Aspects of Electrochemistry, vol. 35. The electroless deposition itself is quite suitable for the production of different structures and materials discussed in the previous chapters of this volume. If properly carried out, this simple process produces very uniform and continuous coatings on complex shapes, which are difficult to obtain by other competitive technologies. The electroless deposition is used in many areas of production of modern materials and devices. Recent advances in electronics, energy conversion, biomedical fields, etc. are presented. For the successful operation of electroless deposition on the industrial scale, the basic mechanistic aspects should further be investigated.

This new volume of Modern Aspects of Electrochemistry brings to the scientists, engineers, and students new concepts and summarized results in the field of science of electrochemical and chemical deposition, which may have significant influence for future practical applications.

Stojan S. Djokić
Edmonton, AB

Contents

Preface v

Contributors xv

Chapter 1

HYDROGEN CO-DEPOSITION EFFECTS
ON THE STRUCTURE OF ELECTRODEPOSITED COPPER

Nebojša D. Nikolić and Konstantin I. Popov

I. Introduction 1
II. The Concept of "The Effective Overpotential" 4
1. The Definition of the Concept and Mathematical Model 4
2. The Concept of "Effective Overpotential" Applied for Metal Electrodeposition Under an Imposed Magnetic Field 14
III. Phenomenology of a Formation of a Honeycomb-Like Structure During Copper Electrodeposition 17
IV. The Effect of Deposition Conditions on Copper Deposits Morphology 24
1. The Surface Preparation 24
2. The Effect of Concentration of Cu(II) Ions 26
(i) Morphologies of Copper Deposits Obtained at Overpotentials up to 800 mV 32
(ii) Morphologies of Copper Deposits Obtained at an Overpotential of 1,000 mV 35
3. The Effect of Concentration of H_2SO_4 41
(i) Morphologies of Copper Deposits Obtained at Overpotentials up to 800 mV 44
(ii) Morphologies of Copper Deposits Obtained at an Overpotential of 1,000 mV 48

4. The Effect of Temperature on Electrodeposition of Disperse Copper Deposits 49
5. Analysis of Deposition Conditions with the Aspect of the Honeycomb-like Structure Formation 55
V. Influence of Ionic Equilibrium in the $CuSO_4$–H_2SO_4–H_2O System on the Formation of Irregular Electrodeposits of Copper 59
VI. The Shape of Electrochemically Formed Copper Powder Particles and their Dependence on the Quantity of Evolved Hydrogen 62
Acknowledgment 67
References 67

Chapter 2

NOBLE METAL NANOISLANDS DECORATION OF AU(111) AND PT(111) SINGLE CRYSTAL SURFACES

Svetlana Strbac and Andrzej Wieckowski

I. Introduction 71
II. Preparation and Characterization of Me/Au(111) and Me/Pt(111) Surfaces 73
1. Au(111) and Pt(111) Single Crystal Preparation for In Situ STM Measurements 73
2. In Situ STM Imaging of the Au(111) and Pt(111) Single Crystals Decorated with Metal Nanoislands . 76
III. Electrochemical Deposition of Ru on Au(111) 77
1. The Electrodeposition of Ru on Au(111) Observed by Cyclic Voltammetry 77
2. The Electrodeposition of Ru on Au(111) Observed by In Situ STM 80
IV. Spontaneous Deposition of Ru on Au(111) 84
V. Spontaneous Deposition of Os on Au(111) 90
VI. Spontaneous Deposition of Ru on Pt(111) 96
VII. Spontaneous Deposition of Os on Pt(111) 98
VIII. Applications of Selected Bimetallic Surfaces for the Electrocatalytic Purposes 101
1. CO Oxidation on Ru/Au(111) Prepared by Electrochemical Ru Deposition 101

2. CO Oxidation on Ru/Au(111) Prepared by Spontaneous Ru Deposition 103
3. Formaldehyde Oxidation on Ru/Au(111) Prepared by Spontaneous Ru Deposition 104
4. CO Oxidation on Os/Au(111) Prepared by Spontaneous Os Deposition 107
5. CO Oxidation on Ru/Pt(111) Prepared by Spontaneous Ru Deposition 107
6. Methanol Oxidation on Pt(111) Modified by Spontaneously Deposited Ru 109
7. CO Oxidation on Os/Pt(111) Prepared by Spontaneous Os Deposition 111
IX. Conclusions 112
Acknowledgments 114
References 114

Chapter 3

ELECTRODEPOSITION FOR ELECTROCHEMICAL ENERGY CONVERSION AND STORAGE DEVICES

Nima Shaigan

I. Introduction 117
II. Proton Exchange Membrane Fuel Cells 118
1. Membrane Electrode Assembly 118
2. Electrodeposition of Pt Electrocatalysts for MEAs 119
3. Electrodeposition of Carbon Monoxide Tolerant Electrocatalysts 123
III. Solid Oxide Fuel Cells 125
1. Ferritic Stainless Steel Interconnects for SOFCs 126
2. Conductive/Protective Coatings for Ferritic Stainless Steel Interconnects 126
3. Spinel Coating via Electrodeposition/Heat Treatment 127
(i) Drawbacks of Spinel Coatings via Electrodeposition/oxidation 129
4. Anodic Deposition of Co–Mn Spinels 132

IV. Electrochemical Supercapacitors 133
1. Faradic and Non-Faradic Supercapacitors 133
2. Metal Oxide Electrodes 134
3. Electrodeposition of Manganese Oxides 135
4. Conductive Polymer Electrodes 138
5. Electrodeposition of Conductive Polymers 138
6. Composite Electrodeposition of Metal Oxides/Polymers 144
V. Lithium Ion Batteries 146
1. Tin-Oxide-Based Anodes 147
2. Tin and Tin Intermetallic Anodes 151
VI. Conclusions 154
Acknowledgments 155
References 155

Chapter 4

THE EFFECT OF MORPHOLOGY OF ACTIVATED ELECTRODES ON THEIR ELECTROCHEMICAL ACTIVITY

Konstantin I. Popov, Predrag M. Živković, and Nebojša D. Nikolić

I. Introduction 163
II. Micro- and Macroelectrodes 165
III. Inert Macroelectrode Partially Covered With Hemispherical Active Microelectrodes 171
1. Mathematical Model 171
2. Polarization Curves 176
(i) Calculated Polarization Curves Without Included Ohmic Potential Drop 176
(ii) Calculated Polarization Curves With Included Ohmic Potential Drop 180
3. Experimental Verification 183
4. The Required Quantity of Active Substance 188
IV. Inert Electrodes Activated With Dendrites 190
1. Large Level of Coarseness 190
2. Low Level of Coarseness 198
V. Applied Aspects 208
VI. Conclusions 209

Acknowledgments 210
References 210

Chapter 5

ELECTROCHEMICAL MICROMACHINING AND MICROSTRUCTURING OF ALUMINUM AND ANODIC ALUMINA

Dmitri A. Brevnov and Peter Mardilovich

I. Introduction 215
II. Electrochemical Micromachining and Localized Anodization 217
1. Electrochemical Methods for 3D Microstructure Fabrication: Additive Plating and Wet Subtractive Etching 217
2. Fabrication of 3D Metallic and 3D Ceramic Microstructures Based on Electrochemical Micromachining of Al 218
3. Undermask Anodization During Localized Anodization of Al and Fidelity of the Mask Transfer 219
4. Technological Limitations and Economical Benefits of Electrochemical Micromachining of Al . 221
III. Technological Aspects of Localized Anodization of Aluminum Substrates 222
1. Mask Reliability During Localized Anodization 222
2. Etch Factor as a Function of Process Conditions 224
3. Current Density Distribution at the Pattern Scale During Localized Anodization 228
IV. Localized Anodization and Electrochemical Micromachining: Applications and Devices 231
1. Metallization Applications in the Microelectronics and Solar Cells Industry, and Fabrication of Passive Components 232
2. Surface Microstructuring 235
3. Freestanding Porous Al_2O_3 Substrates and Devices . 239
4. Multilevel Alumina Ceramics and Its Applications . 242

V. Conclusions 245
Acknowledgments 246
References 246

Chapter 6

ELECTROLESS DEPOSITION: THEORY AND APPLICATIONS

Stojan S. Djokić and Pietro L. Cavallotti

I. Introduction 251
II. General Considerations of Electroless Deposition 252
1. Displacement Deposition 253
2. Autocatalytic Deposition 256
3. Electroless Oxidation of Metals 261
III. Mechanistic Aspects Of Electroless Deposition 262
IV. Recent Developments and Applications of Electroless Deposition 266
1. Electroless Deposition in Electronics Applications . 266
2. Electroless Deposition for Electromagnetic Shielding 272
3. Electroless Deposition of Magnetic Materials 273
4. Electroless Deposition for Energy Conversion and Catalytic Purposes 275
5. Electroless Deposition for the Biomedical Applications 278
6. Electroless Deposition and Anticorrosion Applications 281
7. Electroless Deposition and Nanotechnology 283
V. Conclusions 285
Acknowledgments 286
References 286

Index 291

List of Contributors, MAE 48

Dmitri A. Brevnov
Applied Materials Inc., 3330 Scott Blvd., Santa Clara, CA 95054, USA, dmitri_brevnov@amat.com

Pietro L. Cavallotti
CMIC "G.Natta" Department, Politecnico, Via Mancinelli, 7, Milano, Italy, pietro.cavallotti@polimi.it

Stojan S. Djokić
Elchem Consulting Ltd., Edmonton, AB, Canada T5X 6B3, sdjokic@telus.net

Peter Mardilovich
Hewlett-Packard Company, 1000 NE Circle Blvd, Corvallis, OR 97330, USA, peter.mardilovich@hp.com

Nebojša D. Nikolić
ICTM – Institute of Electrochemistry, University of Belgrade, Njegoseva 12, POB 473, 11001 Belgrade, Serbia, nnikolic@tmf.bg.ac.rs

Konstantin I. Popov
Faculty of Technology and Metallurgy, University of Belgrade, Karnegijeva 4, POB 3503, 11001 Belgrade, Serbia, kosta@tmf.bg.ac.yu

Nima Shaigan
NRC Institute for Fuel Cell Innovation, 4250 East Mall, Vancouver, BC, Canada V6T 1W5, nima.shaigan@nrc-cnrc.gc.ca

Svetlana Štrbac
ICTM – Institute of Electrochemistry, University of Belgrade, Njegoseva 12, POB 473, 11001 Belgrade, Serbia, sstrbac@elab.tmf.bg.ac.rs

Andrzej Wieckowski
Department of Chemistry, University of Illinois, Urbana, IL, USA, andrzej@scs.uiuc.edu

Predrag M. Živković
Faculty of Technology and Metallurgy, University of Belgrade, Karnegijeva 4, POB 3503, 11001 Belgrade, Serbia, peca@tmf.bg.ac.rs

Modern Aspects of Electrochemistry

Topics in Number 45 include:

- The cathodic reduction of nitrate and electrochemical membrane technology
- Non-haloaluminate ionic liquids
- The properties of nanowires composed of metals and semiconductors.
- Ammonium electrolysis as a renewable source of fuel
- The usefulness of synchrotron x-ray scattering to a wide range of electrode phenomena

Topics in Number 46 include:

- Comprehensive review of the structural aspects and anti-corrosion properties of passive films on metals and alloys
- Research on nano- and micro-fabrications based on anodizing treatments combined with chemical/mechanical processes such as laser irradiation, atomic force micro-probe processing and thin film deposition techniques
- Passivity of aluminum-based amorphous alloys and stainless steels and the catalytic activity of copper-based amorphous alloys
- Theoretical analysis of the admittance behavior of passive film/electrolyte junction based on the theory of amorphous semiconductor Schottky barriers

1

Hydrogen Co-deposition Effects on the Structure of Electrodeposited Copper

Nebojša D. Nikolić[1] and Konstantin I. Popov[1,2]

[1] *ICTM-Institute of Electrochemistry, University of Belgrade, Njegoševa 12, Belgrade, Serbia*
[2] *Faculty of Technology and Metallurgy, University of Belgrade, Karnegijeva 4, Belgrade, Serbia*

I. INTRODUCTION

The creation of open porous structures with an extremely high surface area is of great technological significance because such structures are ideally suited for electrodes in many electrochemical devices, such as fuel cells, batteries, and chemical sensors.[1] The open porous structure enables the fast transport of gases and liquids, while the extremely high surface area is desirable for the evaluation of electrochemical reactions. The electrodeposition technique is very suitable for the preparation of such structures because it is possible to control the number, distribution, and pore size in these structures by the choice of appropriate electrolysis parameters.

These metal structures can be formed in both potentiostatic and galvanostatic regimes of electrolysis and their formation are always accompanied by strong hydrogen co-deposition. Hydrogen evolution is the second reaction which occurs at the cathode during electrodeposition processes from aqueous solutions; in some cases it can be

S.S. Djokić (ed.), *Electrodeposition: Theory and Practice*,
Modern Aspects of Electrochemistry 48, DOI 10.1007/978-1-4419-5589-0_1,

ignored while in other cases it cannot.[2] Co-deposition of hydrogen during chromium electroplating is the best documented system,[3,4] because the cathode current efficiency for chromium electrodeposition is 10–25%. Generally, the effect of hydrogen co-deposition during metal electrodeposition processes can be manifested through:[2]

1. Hydrogen absorption which occurs in the substrate metal as H atoms, not H_2 molecules, but may gather as molecule bubbles in voids or vacancies, thus leading to hydrogen embrittlement.
2. Hydrogen bubbles which cling to the surface in an adsorbed state; this leads to the growth of pores as the deposition continues around the bubbles before they are released.
3. Hydrogen bubble evolution can provide a stirring effect and lead to a substantial bubble raft at the free surface of the solution.

The most often employed electrolytes for the electrodeposition of copper are those based on aqueous solutions of sulfuric acid (H_2SO_4) and cupric sulfate ($CuSO_4$).[5] The main species present in aqueous sulfuric acid solutions containing Cu(II) are: bisulfate ions (HSO_4^-), cupric ions (Cu^{2+}), aqueous cupric sulfate ($CuSO_{4(aq)}$), hydrogen ions (H^+), and sulfate ions (SO_4^{2-}).[6–8] In an aqueous solution of sulfuric acid and cupric sulfate, two weak electrolytes, HSO_4^- and $CuSO_{4(aq)}$, are formed according to the following reactions:

$$H^+ + SO_4^{2-} \rightleftarrows HSO_4^- \quad (1)$$

$$Cu^{2+} + SO_4^{2-} \rightleftarrows CuSO_{4(aq)} \quad (2)$$

Pitzer's model[9] was used to calculate the ionic equilibrium in the $CuSO_4$–H_2SO_4–H_2O system over a wide range of concentrations and temperatures.[8] Using Pitzer's model, the relative concentrations of hydrogen ions (H^+) as a function of the total copper concentration and solution acidity were calculated, and this dependence is presented in Fig. 1. From Fig. 1 it can be clearly seen that increasing the copper concentration produces a sharp decrease in the hydrogen ion concentration, while increasing the concentration of sulfuric acid produces an increase in the hydrogen ion concentration.

According to (1) and (2), the addition of sulfuric acid to the solution decreases the concentration of free sulfate ions due to the

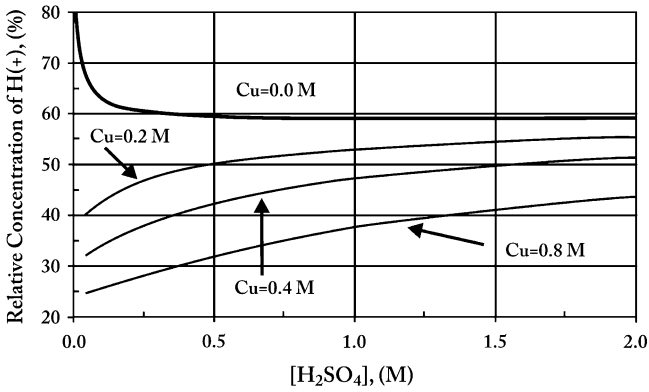

Figure 1. Relative concentration of hydrogen ions as function of sulfuric acid and total copper concentrations, at 25°C ($C_{RH+} = [H^+]/[H_T]$). (Reprinted from Ref. [8] with permission from Elsevier).

formation of bisulfate ions. The addition of cupric sulfate to the solution increases the concentration of bisulfate ions and decreases the concentration of hydrogen ions.

In the case of copper electrodeposition,[10] as opposed to other metals such as nickel and cobalt,[11,12] there are well-defined ranges of current densities and overpotentials without and with hydrogen co-deposition. The beginning of the hydrogen evolution reaction, as the second reaction, corresponds to some overpotential belonging to the plateau of the limiting diffusion current density, being higher than the critical overpotential for the initiation of dendritic growth and lower than that for instantaneous dendritic growth.[13] Increasing the overpotential intensifies the hydrogen evolution reaction and at some overpotential outside the plateau of the limiting diffusion current density, hydrogen evolution becomes vigorous enough to change the hydrodynamic conditions in the near-electrode layer. This offers the possibility of detailed investigations and comparison of the morphologies of copper, and consequently, of any other metals, obtained without and with hydrogen co-deposition.

In the case of copper, electrodeposition at low overpotentials produces large grains with relatively well-defined crystal shapes. Further increasing the overpotential leads to the formation of cauliflower-like and carrot-like protrusions, and finally, dendritic deposits are formed in the absence of strong hydrogen co-deposition.[13]

Strong hydrogen co-deposition leads to a mixing of the solution and changes the mass transfer limitations at an electrode surface. At the same time, the evolved hydrogen bubbles exert substantial effects on mass and heat transfer, limiting current density and ohmic resistance,[14–16] as well as on the morphology of the deposit, leading to the formation of open porous structures with an extremely high surface area.[1,10,17–19]

Electrodeposition of copper under conditions of a vigorous hydrogen co-deposition is of high technological significance, because open porous structures of copper with an extremely high surface area are suitable for the construction of nanocomposite anodes (consisting of Cu and CeO_2) for solid oxide fuel cells.[1] Also, copper shows a high activity for nitrate ion reduction,[20] as well as for a reaction in which nitrate is reduced to ammonia in high yield in aqueous acidic perchlorate and sulfate media.[21]

Bearing in mind the great practical significance of copper deposits obtained under the conditions of hydrogen co-deposition, as well as the fact that detailed investigations at high current densities and overpotentials have been performed only from the point of view of the formation of metal powders,[13,22–25] a better understanding of the effect of hydrogen evolution on the electrodeposition of copper at high overpotentials is necessary.

The morphology of electrodeposited copper in the presence of vigorous hydrogen evolution was described recently,[1] and the mechanism of the formation of this type of morphology was established by Nikolić et al.[10]

The aim of this chapter was to give comprehensive treatment of the morphology of copper electrode posited at high overpotentials, especially in the presence of hydrogen co-deposition, obtained in the potentiostatic conditions from different electrolytes and at different temperatures.

II. THE CONCEPT OF "THE EFFECTIVE OVERPOTENTIAL"

1. The Definition of the Concept and Mathematical Model

The polarization curve for copper electrodeposition from 0.15 M $CuSO_4$ in 0.50 M H_2SO_4 is shown in Fig. 2. The average current efficiencies for hydrogen evolution reaction, $\eta_{av}(H_2)$, in potentiostatic

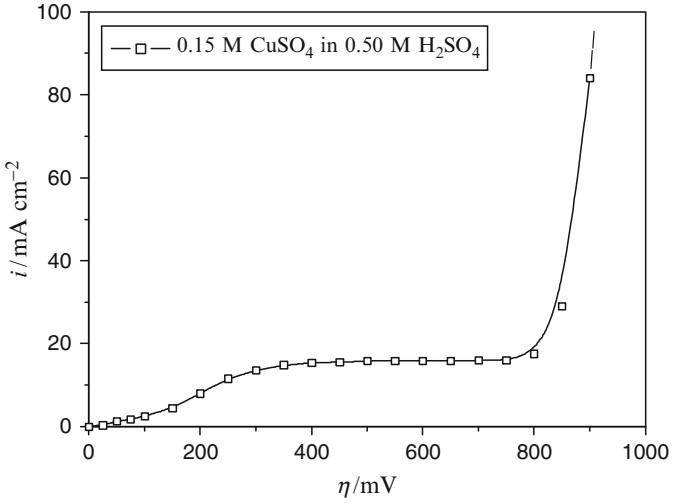

Figure 2. Polarization curve for the cathodic process of copper deposition from 0.15 M $CuSO_4$ in 0.50 M H_2SO_4. Temperature: 18.0 ± 1.0°C. (Reprinted from Ref. [10] with permission from Elsevier).

deposition are derived from the dependences of the current of copper electrodeposition on time and the dependences of the volume of the evolved hydrogen on time[10] using procedure described in Ref. [26]

The average current efficiency for hydrogen evolution reaction at an overpotential of 700 mV was very small (near 2.0%),[10] and at lower overpotentials it even cannot be observed. The average current efficiency for the hydrogen evolution at an overpotential of 800 mV was 10.8%, while at an overpotential of 1,000 mV was 30.0%.[10] The critical overpotential for the beginning of the hydrogen evolution can be estimated to be about 680 mV.[10]

The morphologies of copper electrodeposits obtained potentiostatically, onto vertical stationary copper wire electrodes previously covered by copper thin films[10] from a copper solution containing 0.15 M $CuSO_4$ in 0.50 M H_2SO_4, at a temperature of 18.0 ± 1.0°C in different hydrogen co-deposition conditions are shown in Figs. 3–10.

The deposits obtained at an overpotential of 550 mV with different quantities of electricity are shown in Figs. 3–6. At this overpotential, there is no hydrogen co-deposition at all. The deposit obtained with a quantity of electricity of 2.5 mA h cm^{-2} is shown

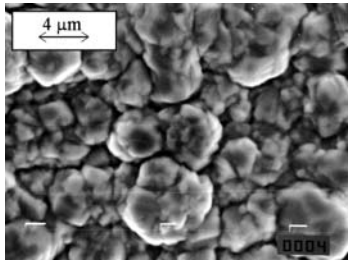

Figure 3. Copper deposit obtained at an overpotential of 550 mV. Quantity of electricity: 2.5 mA h cm^{-2}. (Reprinted from Ref. [10] with permission from Elsevier).

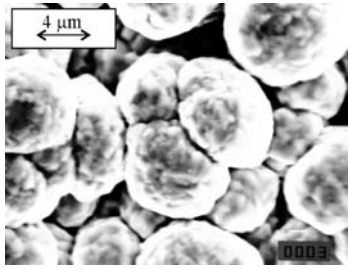

Figure 4. Copper deposit obtained at an overpotential of 550 mV. Quantity of electricity: 5.0 mA h cm^{-2}. (Reprinted from Ref. [10] with permission from Elsevier).

in Fig. 3. The surface film is completed, the grains grown by electrodeposition on the initially formed nuclei practically touch each other and there is no new nucleation on already existing grains. The difference in size between grains can also be observed. This is due to the fact that the nucleation does not occur simultaneously over the whole cathode surface, but it is a process extended in time, so that crystals generated earlier may be considerably larger in the size than ones generated later. These differences increase with an increased quantity of electrodeposited metal, what can be seen from Fig. 4 presenting the copper deposit obtained with a quantity of

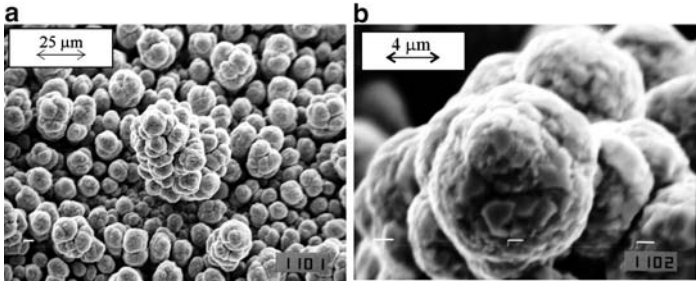

Figure 5. Copper deposit obtained at an overpotential of 550 mV: (**a**) cauliflower-like structure, and (**b**) the detail from Fig. 5a. Quantity of electricity: 10 mA h cm^{-2}. (Reprinted from Ref. [10] with permission from Elsevier).

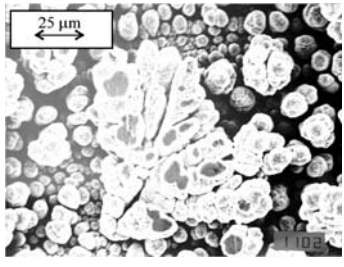

Figure 6. Copper deposit obtained at an overpotential of 550 mV. Quantity of electricity: 20 mA h cm^{-2}. (Reprinted from Ref. [17] with permission from Elsevier).

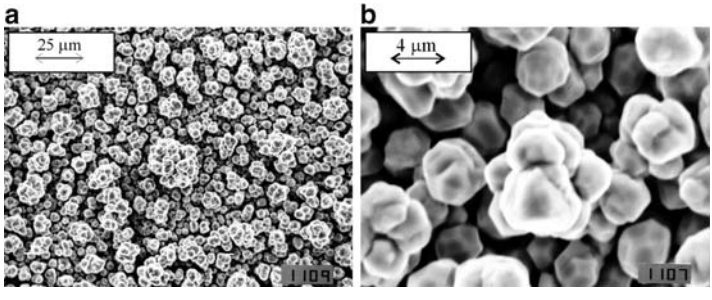

Figure 7. Copper deposit obtained at an overpotential of 700 mV: (**a**) cauliflower-like structure, and (**b**) the detail from Fig. 7a. Quantity of electricity: 2.5 mA h cm^{-2}. (Reprinted from Ref. [10] with permission from Elsevier).

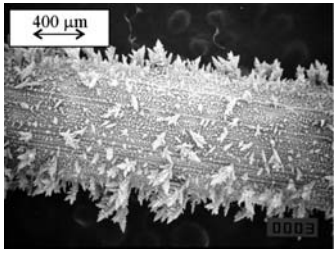

Figure 8. Copper deposit obtained at an overpotential of 700 mV. Quantity of electricity: 5.0 mA h cm^{-2}. (Reprinted from Ref. [10] with permission from Elsevier).

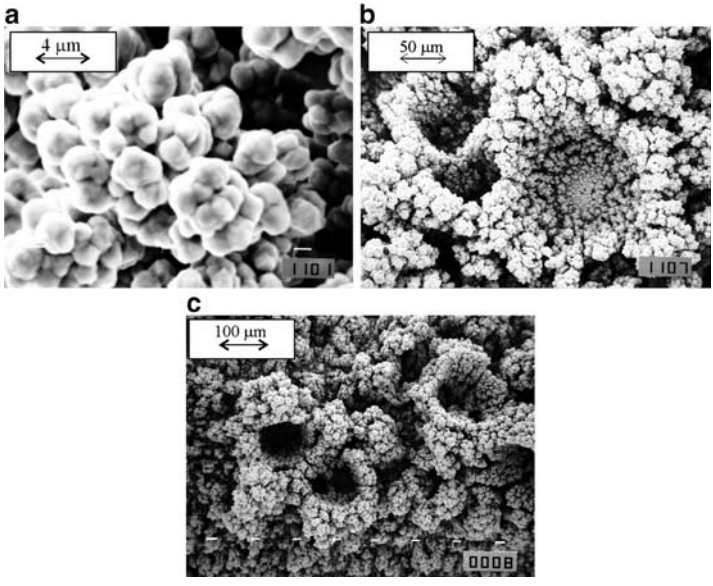

Figure 9. Copper deposit obtained at an overpotential of 800 mV. (**a**, **b**) quantity of electricity: 5.0 mA h cm^{-2} and (**c**) quantity of electricity: 10 mA h cm^{-2}. (Reprinted from Ref. [10] with permission from Elsevier).

electricity of 5.0 mA h cm^{-2}. These enlarged differences are also the consequence of the fact that some smaller grains are consumed by the larger ones,[27] as can be deduced from Figs. 3 and 4. This is also illustrated by Fig. 5a. The increase of the quantity of the

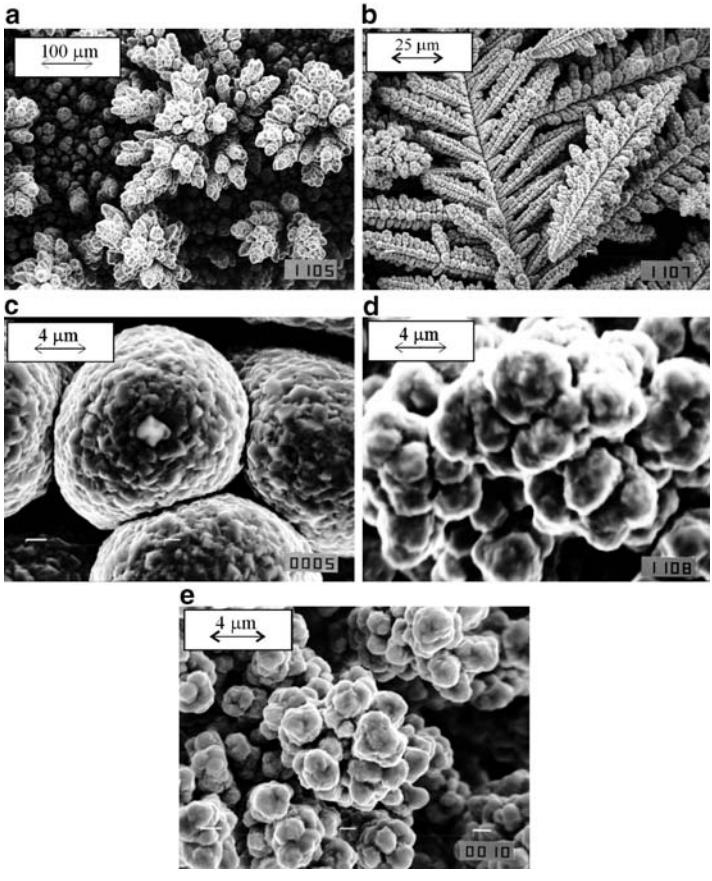

Figure 10. Copper deposits obtained with a quantity of the electricity of 20 mA h cm^{-2} and at overpotentials of: (**a**) 550 mV, (**b**) 700 mV, (**c**) 450 mV, (**d**) 800 mV, and (**e**) 1,000 mV. (Reprinted from Ref. [10] with permission from Elsevier).

electrodeposited metal led to the formation of a cauliflower-like structure (Fig. 5a, b). Furthermore, from Fig. 5a it can be seen that the spherical diffusion layers inside linear diffusion layer of the macroelectrode are formed around these cauliflower-like particles. Finally, further increase of the quantity of the electrodeposited metal produces dendritic deposit (Fig. 6).

On the other hand, it is well known that the induction time of dendrite growth initiation strongly decreases with increasing overpotential of electrodeposition.[28] The situation on the electrode surface after deposition with 2.5 mA h cm^{-2} at 700 mV (Fig. 7) is very similar to the situation after 10 mA h cm^{-2} at 550 mV (Fig. 5). The most important difference is in the shape and size of growing grains, being less globular and smaller in electrodeposition at 700 mV. Besides, the interparticle distances are relatively equal which indicate that these distances are not due to appearance of hydrogen co-deposition, which is still very small at 700 mV. Dendrites appear at 700 mV after deposition with 5.0 mA h cm^{-2} (Fig. 8).[10]

The electrodeposition at 800 mV with the quantity of the electricity of 5.0 mA h cm^{-2} (Fig. 9) did not lead to the formation of copper dendrites as at previously analyzed overpotential of 700 mV. The agglomerates of small copper grains become dominant form of the copper morphology electrodeposited at this overpotential (Fig. 9a) being similar to that from Fig. 7b. Also, there are large holes or craters between the agglomerates of these grains, which is probably due to the hydrogen co-deposition (Fig. 9b). This copper deposit is denoted as a honeycomb-like structure with craters as main characteristic,[10] as was shown earlier for copper and tin deposits in Ref. [1] The honeycomb-like structure is formed at 800 mV and with twice the quantity of electricity (Fig. 9c), as well as at an overpotential of 1,000 mV.[10] (see also Sect. III).

It is known that the hydrogen evolution effects onto the hydrodynamic conditions inside electrochemical cell.[29–31] The increase in hydrogen evolution rate leads to the decrease of the diffusion layer thickness and, hence, to the increase of limiting diffusion current density of electrode processes. It was shown[29] that if the rate of gas evolution at the electrode is larger than 100 cm^3/cm^2 min (>5 A/cm^2), the diffusion layer becomes only a few micrometers thick. It is also shown[29] that a coverage of an electrode surface with gas bubbles can be about 30%. If the thickness of the diffusion layer in conditions of natural convection is $\sim 5 \times 10^{-2}$ cm and in strongly stirred electrolyte $\sim 5 \times 10^{-3}$ cm,[32] it is clear that gas evolution is the most effective way to decrease mass transport limitations for electrochemical processes in mixed activation – diffusion control.

The overpotential η and the current density i are related by

$$\eta = \frac{b_c}{2.3} \ln \frac{i}{i_o} + \frac{b_c}{2.3} \ln \frac{1}{1 - (i/i_L)}, \tag{3}$$

where i_o, i_L, and b_c are the exchange current density, the limiting diffusion current density and cathodic Tafel slope for electrochemical process in mixed activation – diffusion control.[13] The first term in (3) corresponds to the activation part of deposition overpotential and the second one is due to the mass transfer limitations. If one and the same process takes place under two different hydrodynamic conditions, characterized by two different values of the limiting diffusion current densities $i_{L,1}$ and $i_{L,2}$, (3) can be rewritten in the forms:

$$\eta_1 = \frac{b_c}{2.3} \ln \frac{i_1}{i_o} + \frac{b_c}{2.3} \ln \frac{1}{1 - (i_1/i_{L,1})} \tag{4}$$

and

$$\eta_2 = \frac{b_c}{2.3} \ln \frac{i_2}{i_o} + \frac{b_c}{2.3} \ln \frac{1}{1 - (i_2/i_{L,2})}, \tag{5}$$

where η_1 and η_2 and i_1 and i_2 are the corresponding values of overpotentials and current densities. The same degree of diffusion control is obtained if

$$\frac{i_1}{i_{L,1}} = \frac{i_2}{i_{L,2}} \tag{6}$$

or,

$$i_2 = i_1 \frac{i_{L,2}}{i_{L,1}} \tag{7}$$

and substitution of i_2 from (7) in (5) and further rearranging gives

$$\eta_2 = \frac{b_c}{2.3} \ln \frac{i_1}{i_o} + \frac{b_c}{2.3} \ln \frac{1}{1 - (i_1/i_{L,1})} + \frac{b_c}{2.3} \ln \frac{i_{L,2}}{i_{L,1}} \tag{8}$$

and
if (4) is taken into account:

$$\eta_2 = \eta_1 + \frac{b_c}{2.3} \ln \frac{i_{L,2}}{i_{L,1}}. \tag{9}$$

Hence, if

$$i_{L,2} > i_{L,1} \tag{10}$$

in order to obtain the same degree of diffusion control in two hydrodynamic conditions, (9) must be satisfied, meaning that

$$\eta_2 > \eta_1. \tag{11}$$

The results presented here can be then explained as follows. In the absence of strong hydrogen evolution, the diffusion layer is due to the natural convection and does not depend on the overpotential of electrodeposition. As excepted, for deposition times lower than the induction time for dendritic growth initiation, the same type of deposit at larger overpotential (Fig. 7) is obtained as at lower overpotential (Fig. 5), being somewhat different in grain sizes and particle shapes.

The vigorous hydrogen evolution changes the hydrodynamic conditions and decreases the degree of diffusion control. Hence, (9) should be rewritten in the form:

$$\eta_1 = \eta_2 - \frac{b_c}{2.3} \ln \frac{i_{L,2}}{i_{L,1}}, \tag{12}$$

where η_1 becomes the effective overpotential, $\eta_1 = \eta_{eff}$, related to conditions of natural convection at which there is the same degree of diffusion control as at overpotential η_2 with the hydrogen co-deposition. Hence, the dendritic growth can be delayed or completely avoided, as can be seen from Fig. 9c, meaning that there is a really lower degree of diffusion control at an overpotential of 800 mV with the hydrogen co-deposition than at an overpotential of 700 mV where the hydrogen co-deposition is very small.

Hence, on the basis of presented results, we can propose a concept of "effective overpotential" for a metal electrodeposition. This concept is proposed – thanks to morphologies of copper deposits obtained at high deposition overpotentials (800 mV and more)[10] where the hydrogen evolution occurs. These copper deposits are probably the consequence of the stirring of electrolyte in the near-electrode layer by evolving hydrogen. This process leads to a decrease of the thickness of diffusion layer, and consequently, up to an increase of the limiting current density. According to (12), the increase of the limiting current density leads to a metal deposition at an overpotential, which is effectively lower than the specified one. Then, the obtained morphologies of copper deposits become similar to the ones obtained at some lower overpotential at which the hydrogen co-deposition does not exist.

The better understanding of the concept "effective overpotential" can be realized by taking into account the fact that the time of dendritic growth initiation depends on used deposition overpotentials. Increasing deposition overpotentials lead to decreasing times for

the beginning of dendritic growth.[28] Observing deposits obtained at overpotentials belonging to the limiting diffusion current density plateau (550 and 700 mV), one can notice that cauliflower-like forms are obtained at an overpotential of 550 mV (Fig. 5a), and dendritic forms at an overpotential of 700 mV (Fig. 8). Meanwhile, the electrodeposition with a quantity of the electricity of 20 mA h cm^{-2} leads to the formation of degenerate dendritic structure at 550 mV (Figs. 6 and 10a). Copper dendrites remain a main characteristic of the electrodeposition at 700 mV (Fig. 10b). On the other hand, it can be shown that copper dendrites are not formed by the electrodeposition at lower overpotential (for example, at 450 mV where the hydrogen evolution was also zero) with a quantity of the electricity of 20 mA h cm^{-2} (Fig. 10c). The main forms of the copper deposit obtained at this overpotential are copper globules. Also, dendritic forms are not formed with a quantity of the electricity of 20 mA h cm^{-2} and during electrodepositions at overpotentials of 800 and 1,000 mV (Fig. 10d, e). The agglomerates of copper particles remain the main characteristics of the structure of deposits obtained at these overpotentials. The macromorphology of these deposits will be discussed later.

Anyway, the structure of copper deposits obtained at overpotentials of 800 and 1,000 mV with a quantity of the electricity of 20 mA h cm^{-2} was similar to those obtained at lower overpotentials before the beginning of dendritic growth. The absence of copper dendrites at overpotentials of 800 and 1,000 mV after the electrodeposition with 20 mA h cm^{-2}, as well as the similarity of the obtained morphologies of copper deposits with those obtained at lower overpotentials before dendritic growth initiation clearly indicates that there is really lower degree of diffusion control at these overpotentials than at overpotentials of 550 and 700 mV, respectively.

The concept of "effective overpotential" can be probably applied in other cases where there is a change of hydrodynamic conditions in the near-electrode layer. The change of hydrodynamic conditions, and consequently, of metal morphologies can be caused by stirring of plating solutions in ultrasonic field,[33] in an imposed magnetic field (magnetohydrodynamic effect – MHD effect),[34–39] as well as by stirring of solution by RDE (rotating disk electrode).[40]

2. The Concept of "Effective Overpotential" Applied for Metal Electrodeposition Under an Imposed Magnetic Field

Nickel deposits obtained at a cathodic potential of −1,300 mV/SCE without and with a parallel orientation of magnetic field of 500 Oe, are shown in Fig. 11a, b, respectively. Figure 11a shows that the nickel deposit obtained without an imposed magnetic field consisted of bunch of nickel grains, while it can be seen from Fig. 11b that the nickel deposit obtained under a magnetic field with a parallel orientation to the electrode surface was a porous structure and without bunch of nickel grains.

Figure 12 shows copper deposits obtained at a cathodic potential of −500 mV/SCE without and with a magnetic field of 500 Oe applied to be parallel to the electrode surface. It can be seen from

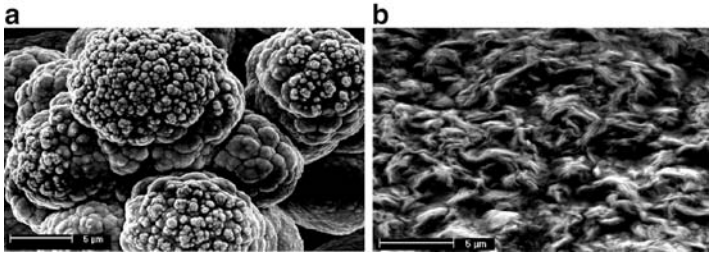

Figure 11. Nickel deposits obtained at a cathodic potential of −1,300 mV/SCE: (**a**) without and (**b**) with a magnetic field of parallel orientation of 500 Oe. (Reprinted from Ref. [39] with permission from the Serbian Chemical Society).

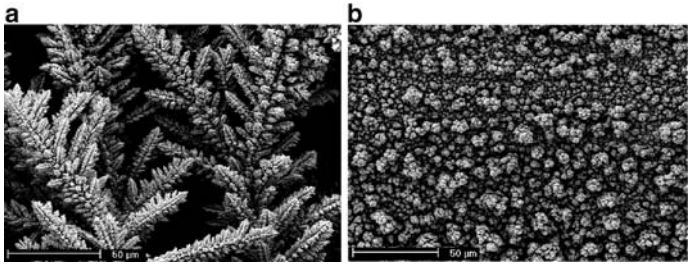

Figure 12. Copper deposits obtained at a cathodic potential of −500 mV/SCE: (**a**) without and (**b**) with a magnetic field of parallel orientation of 500 Oe. (Reprinted from Ref. [39] with permission from the Serbian Chemical Society).